

Detection of trace metals in water by filament- and plasma-grating-induced breakdown spectroscopy

Mengyun Hu,^{a,b,c} Fangfang Li,^{a,b} Shencheng Shi,^{a,b} Yu Qiao,^{a,b} Jinman Ge,^d Xiaojun Li,^d and Heping Zeng^{id a,b,e,f,*}

^aEast China Normal University, State Key Laboratory of Precision Spectroscopy, Shanghai, China

^bChongqing Institute of East China Normal University, Chongqing Key Laboratory of Precision Optics, Chongqing, China

^cUniversity of Shanghai for Science and Technology, School of Optical-Electrical and Computer Engineering, Engineering Research Center of Optical Instrument and System (Ministry of Education), Shanghai Key Laboratory of Modern Optical System, Shanghai, China

^dChina Academy of Space Technology (Xi'an), National Key Laboratory of Science and Technology on Space Microwave, Xi'an, Shaanxi, China

^eShanghai Research Center for Quantum Sciences, Shanghai, China

^fChongqing Institute for Brain and Intelligence, Guangyang Bay Laboratory, Chongqing, China

Abstract. Filament- and plasma-grating-induced breakdown spectroscopy (F-GIBS) was demonstrated as an efficient technique for sensitive detection of metals in water, where plasma gratings were established through synchronized nonlinear interaction of two noncollinear filaments and an additional filament was generated with another fs laser beam propagating along their bisector. A water jet was constructed vertically to the three coplanar filaments, overcoming side effects from violent plasma explosion and bubble generation. Three distinct regimes of different mechanisms were validated for nonlinear couplings of the third filament with plasma gratings. As the third filament was temporally overlapped with the two noncollinear filaments in the interaction zone, all the three filaments participated in synchronous nonlinear interaction and plasma grating structures were altered by the addition of the third filament. As the third filament was positively or negatively delayed, the as-formed plasma gratings were elongated by the delayed third filament, or plasma gratings were formed in the presence of plasma expansion of the ahead third filament, respectively. Using F-GIBS for trace metal detection in water, significant spectral line enhancements were observed.

Keywords: laser-induced breakdown spectroscopy; filament and plasma-gratings induced breakdown spectroscopy; filaments; plasma gratings; grating induced breakdown spectroscopy.

Received Jun. 27, 2022; revised manuscript received Oct. 12, 2022; accepted for publication Nov. 8, 2022; published online Jan. 3, 2023.

© The Authors. Published by SPIE and CLP under a Creative Commons Attribution 4.0 International License. Distribution or reproduction of this work in whole or in part requires full attribution of the original publication, including its DOI.

[DOI: [10.1117/1.APN.2.1.016008](https://doi.org/10.1117/1.APN.2.1.016008)]

1 Introduction

Laser-induced breakdown spectroscopy (LIBS) is a well-developed technique that relies on direct measurements of spectral line emissions from laser-induced plasma. Compared with other techniques, such as atomic absorption spectroscopy and inductively coupled plasma emission spectroscopy, LIBS can facilitate convenient, remote, fast, noncontact, and reliable *in situ* measurements of sample contents and concentrations,^{1–5} which has been widely applied for trace element analyses in gas,^{6,7} liquid,^{8–15} or solid^{16–21} samples. Nevertheless, as LIBS is implemented in

aqueous solutions, there still exist great challenges in steering efficient laser ablation to generate plasmas of sufficiently long lifetimes as well as enhancing plasma excitations to improve detection sensitivities. For instance, water pollution control demands *in situ* detection of water pollutants (such as heavy metal elements) at least at ppm level, whereas LIBS techniques developed so far hardly support such requisite *in situ* detection sensitivity. The main bottlenecks include inefficient laser plasma generation in water and its marginal detection sensitivity as well. Typically, LIBS in aqueous solutions is realized by focusing ablating laser pulses inside liquids or on the liquid surfaces. An intrinsic limitation comes from shockwave generation accompanying laser ablation, which unavoidably produces

*Address all correspondence to Heping Zeng, hpzeng@phy.ecnu.edu.cn

microbubbles²² that may cause not only detrimental plasma instabilities but also serious scattering of plasma emissions. In addition, laser ablation in solutions is always affected by the surrounding pressure, and laser-generated plasma usually encounters rapid annihilation,²³ resulting in a shortened plasma lifetime and accordingly weakened breakdown of spectral line signals. Various methods including phase transformation^{24–27} and metal substrate assistance^{8,28,29} have been proposed to improve the detection sensitivity of LIBS in solutions. The drawbacks that restrict directly analyzing liquids could also be partially subdued by dual-pulse LIBS (DP-LIBS) techniques^{30,31} or creating fluid jets.³² Traditional LIBS techniques use nanosecond laser pulses to ablate samples. During their injection upon aqueous surfaces, nanosecond laser pulses usually produce splashes that cause observable laser scattering and thus seriously destroy LIBS detection of aqueous solutions. Plasma shielding effects³³ bring about some additional detriments to laser ablation.

It is well known that high-intensity fs laser pulses undergo filamentation due to automatic balance among intense laser self-focusing, beam diffraction, and defocusing originating from photoionization-generated plasma.^{34,35} The so-called fs filaments have self-guided plasma channels quite attractive for breakdown spectroscopic analyses. Filament-induced breakdown spectroscopy (FIBS)³⁶ has been demonstrated to show superior advantages of stable ablation since the peak intensities are typically clamped at 5×10^{13} W/cm² for filaments in air.^{37,38} Such intensity-clamping nevertheless enforces an unwelcome by-effect on FIBS itself, i.e., a single fs filament cannot surpass the intensity of the FIBS spectral lines beyond the intensity-clamped excitation. FIBS could be in principle applied in aqueous solutions. Particularly, filaments have relatively long channels, and therefore, they enter aqueous solutions immune to aqueous surface wobbling.^{39,40} The main difficulty comes from multifilamentation in aqueous solutions as well as relatively low clamped peak intensities closely related to the large optical nonlinearities of aqueous media.⁴¹ In most cases, single filaments in air randomly break up into multifilaments as they enter aqueous solutions. This weakens plasma excitation. The plasma grating formed by the interaction of two filaments can break through the peak-intensity-clamping effects.^{42–45} Plasma-grating induced breakdown spectroscopy (GIBS) developed by means of noncollinear filament interaction could surmount the peak-intensity-clamped plasma excitations.^{46–49} Further spectral line enhancements were also demonstrated with multidimension plasma-grating induced breakdown spectroscopy (MIBS).^{45,46,50} Interaction of multiple filaments also provides a promising technique to overcome the restrictions of traditional LIBS or FIBS for sensitive detection of aqueous solutions. Grated plasma channels are expected to be immune to aqueous surface wobbling and wavelength-scale microstructures of plasma modulation could be even maintained across the wobbling air–solution interfaces. For verification of its technological effectiveness as well as further developments of its potential applications in detecting aqueous solutions, there remain some intriguing questions deserving further experimental explorations, such as how to overcome side effects from bubble generation induced by plasma gratings,^{51–53} how to increase the plasma excitations dramatically in aqueous solutions, and how to effectively evade random multiple filamentation breakup during filaments passing through air–aqueous interfaces.

In this work, we developed a method to create a stable fluid jet with a small diameter where fs filaments were cross overlapped upon the fluid to form plasma gratings in the plane

vertical to the jet. Instead of using single filaments of <100 μm in diameter, plasma gratings were generated within a relatively large spatial area using nonlinear interaction of noncollinear filaments, facilitating plasma excitation to cover almost the whole jet. Such a small fluid jet and its interaction with spatially large plasma gratings could be easily controlled to make bubbles generated therein expand along the fluid jet, producing negligible influence on plasma-grating ablation that guaranteed quite stable plasma excitations and breakdown emissions. In addition, this interaction protocol supported coupling additional filaments into the plasma gratings. We aligned three noncollinear filaments to interact in a plane vertical to the fluid jet. Since multidimensional plasma gratings face some difficulty in reducing detriments originating from filament induced shockwaves and bubbles,^{52,53} coplanar interaction of multiple filaments, instead of nonplanar filament interaction used in MIBS,⁵⁰ was intentionally used to efficiently control bubble expansion along the fluid jet. As the third filament and plasma gratings were appropriately delayed or synchronized upon the fluid jet, their coplanar nonlinear interactions intriguingly enhanced plasma excitations and elongated the plasma lifetime as well.^{46,50} Rather than a simple combination of FIBS and GIBS, filament- and plasma-grating-induced breakdown spectroscopy (F-GIBS) originated from a conceptually different mechanism involving strong nonlinear couplings of the third filament with plasma gratings. This was verified by experimental measurements on the time evolutions of the plasma gratings and breakdown spectral lines.

2 Experimental Details

2.1 Experimental Setup

The experimental setup was like those used in GIBS⁴⁶ or MIBS,⁵⁰ except that all three fs laser beams were aligned to interact in the same plane. A Ti:S fs laser operated at 800 nm with a maximum pulse energy of 2 mJ and pulse duration of 40 fs was used as the excitation laser source in our experiments. Its repetition rate was fixed at 1 kHz. As single filaments were used to ablate aqueous solutions, the plasma excitation efficiency was quite low, and it was impossible to obtain observable plasma spectral line emissions for trace element analyses. Therefore, we used an auxiliary method of a fluid jet to help improve plasma excitations. As shown in Fig. 1(a), we set up a syringe to form a fluid jet by utilizing the gravity of the water itself and installed a water pump to pump the flowing water back to the syringe so that the fluid jet could form a stable laminar flow. In this way, we avoided the influence of the surface fluctuation of the liquid sample on the spectral line signal and formed a distinct plasma in the excited region. When the fluid jet was ablated with 2D plasma gratings formed by three noncollinear and noncoplanar filaments, violent plasma explosions were normally accompanied to form obvious water splashes to scatter the fluorescence, which not only affected the stability of the plasma-grating induced breakdown but also dramatically reduced the intensities of the plasma spectral line signals. To minimize detrimental influence from plasma explosions, the MIBS setup was modified to sustain noncollinear interactions of three or multiple coplanar filaments. Such noncollinear couplings of coplanar filaments established plasma gratings of 1D microstructures in the common plane rather than formation of 2D plasma gratings used in MIBS.⁵⁰ The schematic of the spatial alignment of the interacting fs pulses is shown in Fig. 1(b). The angle between pulses A and B was 20 deg, and pulse C was aligned to propagate along

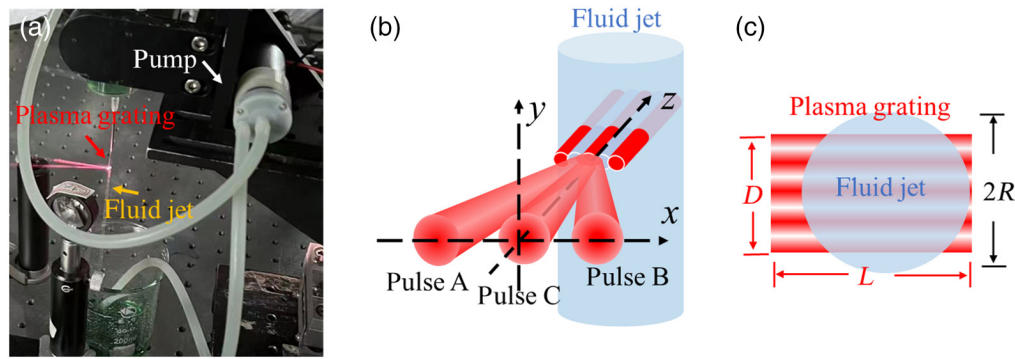


Fig. 1 (a) Photo of plasma-grating excited fluid jet stream. (b) Schematic of the spatial configuration of three filaments generated by pulses A, B, and C. The parallel structure represents plasma gratings generated by the nonlinear interactions of coplanar filaments A, B, and/or C. (c) Schematic of the top view of the plasma grating interacting with the fluid jet.

the bisector of A and B. Pulses A and B were synchronized to form 1D plasma gratings, whereas pulse C was adjusted by means of a delay stage to reach the plasma-grating region with a positive or negative delay, corresponding to pulse C propagating behind or ahead of the synchronized pulses A and B, respectively. Temporal and spatial overlapping of three filaments was aligned as follows. At first, we cross-overlapped filaments A and B in space (with a cross angle of 20 deg) and then scanned the time delay between the two filaments. By monitoring the plasma fluorescence from the side of the plasma channels, we determined the temporally overlapping position as the plasma fluorescence reached its maximum. Plasma gratings were generated as the two filaments underwent nonlinear interactions. Afterward, the third filament (C) was steered in the same plane to propagate along the bisector of filaments A and B. We spatially cross overlapped the third filament with filaments A and B and adjusted their relative time delay. Temporal synchronization of the third filament with the as-formed plasma gratings was determined by monitoring the enhancement of the plasma fluorescence induced by the third filament to reach its maximum. By adjusting the three-dimensional position of the fluid jet, we could realize that part of the plasma gratings was formed in air before they entered the fluid jet,⁴¹ as schematically shown in Fig. 1(c). It should be noted that the plasma gratings were established in the area where two filaments cross-overlapped and interfered. Accordingly, the as-formed plasma gratings typically had a length L significantly shorter than single filaments. Based on the typical filament diameter of $100\ \mu\text{m}$ in air and the angle between the interacting filaments A and B, it could be easily calculated that plasma grating modulation covered a width D slightly smaller than the fluid jet diameter $2R$ [as denoted in Fig. 1(c)]. In addition, filaments and plasma gratings reached their automatic balance between Kerr self-focusing and plasma defocusing. Single fs pulses underwent filamentation in the region where they were focused to reach the so-called self-focusing thresholds, whereas two synchronized fs pulses interfered in their cross-overlapped region, where self-focusing took place along the constructive interference fringes and was then automatically balanced by local plasma defocusing, generating wavelength-scale structures of plasma modulation. Since such interference could in principle enable the self-focusing threshold to be reached in the constructive interference fringes, periodic plasma channels could be established beyond the single

filamentation region as determined by the spatially localized self-focusing along the corresponding interference fringes. Hence, the width [D in Fig. 1(c)] of the plasma gratings became larger than the typical diameters of single filaments. As a result, excitation of plasma gratings could be readily controlled to cover the whole fluid jet. Even though the plasma gratings covered a large area, plasma modulation therein could well confine the laser energies in the wavelength-scale periodic structures and avoid breakup of high-energy filaments into multifilaments especially during their propagation across the air–aqueous interface, and thus more efficient excitation could be achieved in aqueous solutions. Moreover, using plasma gratings with multiple plasma-modulated channels to interact with the aqueous solutions, strong and stable breakdown of spectral lines could be achieved. In our experiments, the signal acquisition mode of the intensified charge-coupled device (ICCD) was set to the so-called on-chip integration mode, and the acquisition gate was set with a width of 500 ns and gate delay of 100 ns. The exposure time of the ICCD was set to 200 ms, corresponding to an accumulation per spectrum of 200 laser shots of ablation with an fs laser of 1 kHz repetition rate used in our experiments.

2.2 Sample Preparation

In our experiments, three kinds of mineral salts with an analytical reagent grade, CuCl_2 , $\text{CrCl}_3 \cdot 6\text{H}_2\text{O}$, and NaCl (all from Sinopharm Chemical Reagent Co., Ltd.) were used. They were dissolved together in deionized water with a concentration of 500 mg/L for each mineral salt. The concentrations of analytical metal elements were thus in 237 ppm for Cu, 97 ppm for Cr, and 196 ppm for Na, respectively. The configured solution was stirred on a magnetic stirrer at 600 rad/s for 5 min and mixed uniformly.

3 Results and Discussions

3.1 Time Evolution of the F-GIBS Spectrum

Figure 2(a) shows the variation trend of the F-GIBS full spectrum with the acquisition gate delay. It can be seen from Fig. 2(a) that in the early stage of plasma formation, the plasma emission involved strong continuous background signals from free electron recombination (free-bound emission) and bremsstrahlung radiation (free-free emission). On the continuous

background signals, there were emission lines of neutral atoms and ions. In the range from 0 to 200 ns, with the increase of the detection delay, the continuous background signals rapidly dropped to negligible, and the spectral line signals emitted by atoms or ions became sharp. However, in the range from 200 to 400 ns, the spectral line signals emitted by atoms or ions continued to decrease as the detection delay was prolonged, which was not conducive to analysis. Therefore, there existed an optimal detection delay. We selected Cu I 324.7 nm to optimize the detection delay. The variation trend of the intensity and signal-to-noise ratio (SNR) of this spectral line with the detection delay is shown in Fig. 2(b). It is obvious from Fig. 2(b) that the intensity of the spectral line decayed exponentially with the increase of detection delay, but the SNR showed a trend of increasing first and then decreasing. The optimal spectral line SNR occurred when the detection delay was 100 ns. In addition, under this detection condition, the relative standard deviations of the obtained five spectral line intensities were around 3% to 5%. The stable and reproducible spectral line evidenced that our proposed F-GIBS scheme greatly improved the plasma excitation and removed detrimental effects of bubbles caused by plasma explosions in the liquid as expected.

3.2 Nonlinearly Coupled Excitations with Filament and Plasma Gratings

In order to establish efficient plasma excitations, the F-GIBS protocol should be optimized by carefully adjusting the interpulse delay between the third filament formed by pulse C and the plasma gratings formed by pulses A and B. Negative interpulse delay refers to that pulse C excited the sample ahead of the plasma gratings, and vice versa is positive interpulse delay.

Figure 3 shows the variation trend of the intensities of the spectral lines Cu I 324.7, Cr I 425.4, and Na I 588.9 nm with the interpulse delay. Unlike traditional DP-LIBS, which typically showed the time evolution lasting tens of microseconds through plasma expansion and cooling or reheating,^{30,31} the spectral line intensity of F-GIBS changed with the interpulse delay via “M-type” intensity-variation trends within typical durations of a few hundred picoseconds, and reaching their maxima as the delay was about ± 50 ps. Such optimum interpulse delays involved in F-GIBS, at least 5 to 6 orders of magnitudes shorter than that in the nanosecond DP-LIBS,^{30,31}

was comparable to the typical lifetimes of the plasma gratings and plasma in filaments.⁵⁴ Within such ultrashort time delays, there existed observable nonlinear interaction between the plasma gratings and the third (synchronized, ahead, or delayed) filaments. It is interesting to note that the plasma excitations and breakdown spectral line emissions manifested intrinsically different mechanisms for plasma gratings interacting with synchronized, ahead, or delayed filaments, respectively.

Figure 4 shows the top view of the noncollinear interaction area between pulses A and B to create plasma gratings without [Fig. 4(a)] and with [Fig. 4(b)] the third filament (pulse C) entering the plasma grating at +50 ps delay, respectively. When the interpulse delay was 50 ps, the plasma gratings were formed at first to excite the liquid sample. Both in air and in liquid jets, the laser intensity and electron density exhibited periodic modulations, which allowed the laser energy to be concentrated in the corresponding area, thereby helping to break through the peak-intensity-clamping effect of the fs filament to achieve better ablation.^{52,53} In our experiments, pulse C was aligned to propagate along the bisectors of A and B [see Fig. 1(b), which could be regarded as the zeroth-order Bragg angle]. Bragg diffraction occurred when pulse C propagated through the plasma gratings,⁵⁵ so that its energy was no longer uniformly distributed but exhibited a periodic distribution, which made the pulse directly self-focus along the as-formed plasma gratings.^{52,53} This stands for a novel nonlinear coupling mechanism for the plasma gratings and delayed filaments. That is, the pulse C underwent filamentation by following the same plasma modulation structures of the as-formed plasma gratings. Thereby, even the pulse C itself could experience a breaking-through of the peak-intensity-clamping of single filamentation in air. Within the lifetime of the as-formed plasma gratings, the still-lasted plasma modulation functioned as modulation seeds for the pulse C, and zeroth order Bragg diffraction of the delayed pulse C enforced the as-formed plasma gratings to be regenerated, with plasma density and plasma modulation contrast enhanced therein regeneratively. Such regenerative formation of plasma gratings elongated the as-formed plasma gratings. Intriguingly, this equivalent lifetime-elongation could be implemented repeatedly with multiple pulses of appropriate delays and thus elongated plasma grating excitations, which might produce plasma excitations comparable to long-pulse ablation. Such nonlinear couplings of plasma gratings with multiple delayed

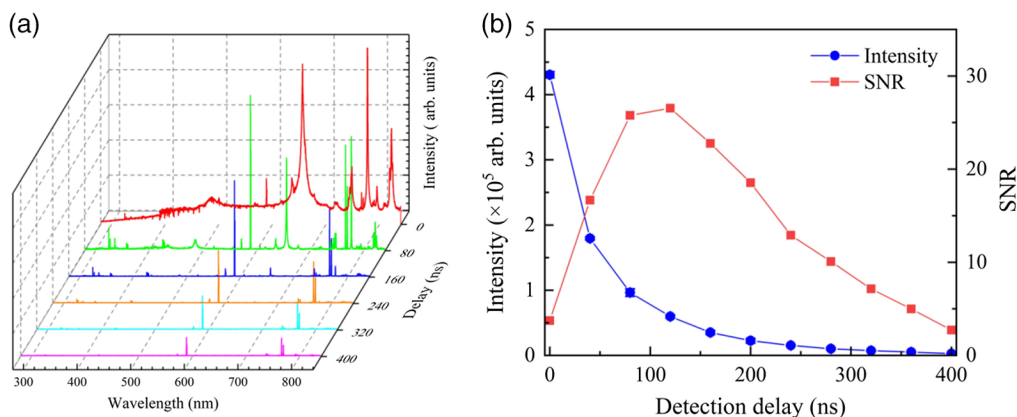


Fig. 2 Time evolution of a typical F-GIBS spectrum: evolution of (a) a typical F-GIBS with the detection delay and (b) the intensity and SNR of Cu I 324.7 nm excited by F-GIBS.

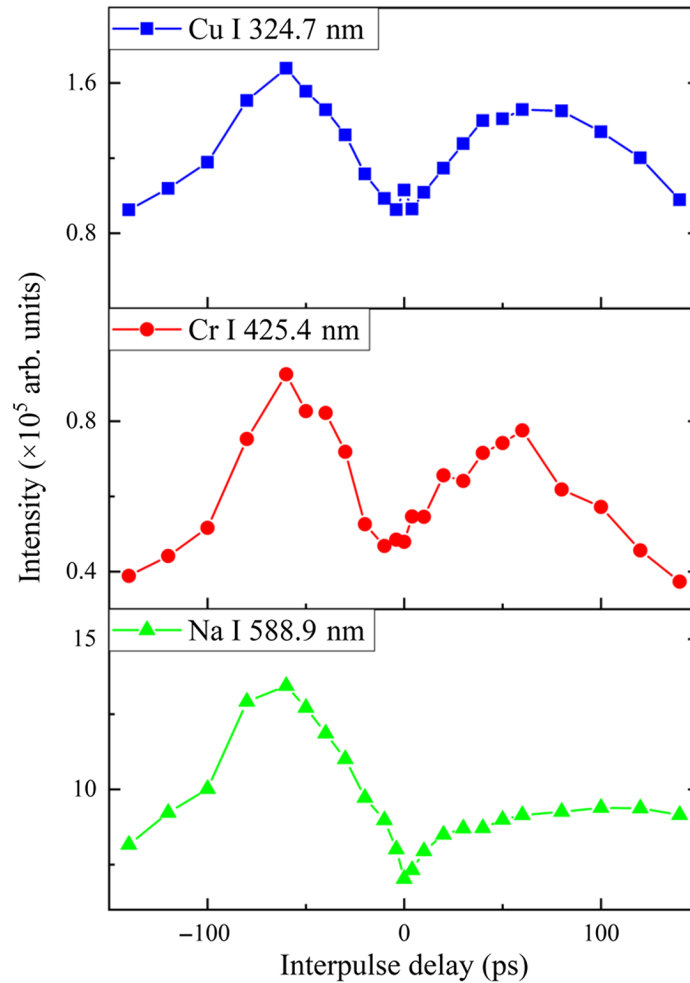


Fig. 3 F-GIBS signals of Cu I 324.7, Cr I 425.4, and Na I 588.9 nm attained under different interpulse delays.

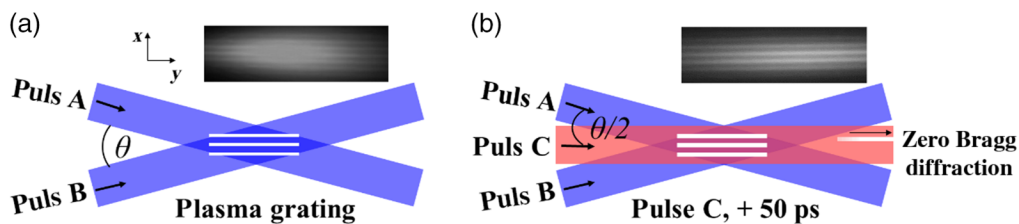


Fig. 4 Top view of the noncollinear interaction area between pulses A and B to create plasma gratings (a) without and (b) with the third filament (pulse C) entering the plasma grating at 50 ps delay, respectively. The plasma grating fluorescence photos are shown in the inset pictures.

pulses inaugurate a technique to overcome the bottleneck intrinsically arisen from the short plasma lifetime of fs filament ablation. As a result, the regenerative formation of plasma gratings benefits to achieve breakdown spectral lines of improved SNRs, better than those excited by the long double pulses used in traditional DP-LIBS,^{56–58} single filaments used in FIBS,^{59–61} or nonregenerative plasma gratings used in GIBS.⁴⁶ Note that such regenerative nonlinear couplings exhibited quite an interesting variation with the delay of the third filaments. At the beginning stage of plasma grating expansion (or plasma modulation decay), pulse C should pass through a plasma background

(nonmodulated plasma generated by pulses A and B) before being coupled into the modulated plasma grating channels, its self-focusing should balance the defocusing arisen from the plasma background of a relatively high plasma density. It has been demonstrated that the plasma expanded faster than the plasma gratings.^{38,40–42,47,48} As the interpulse delay increased, pulse C experienced reduced defocusing losses from the nonmodulated background plasma of rapidly decreased plasma density, and thus it could easily start self-focusing to undergo filamentation, increasing the effective coupling into the long-lasting plasma modulation channels and making the plasma

gratings regenerate with increased efficiencies. The spectral lines attained with such an F-GIBS protocol increased accordingly. Anyhow, the as-formed plasma grating structures also experienced their own decays (although slower than the nonmodulated plasma background), their regenerative nonlinear couplings with the third filament were pronounced only at those delays that there still existed plasma modulation structures. If the third filament were delayed up to a few hundred picoseconds, the as-formed plasma modulations almost disappeared and hence could not be regenerated any longer. Accordingly, the F-GIBS was degraded to double-pulse plasma excitations from the plasma gratings and the delayed filaments without any observable nonlinear couplings. Even under such circumstances, the attained spectral line signals were still much larger than the summation of those attained by the plasma gratings and single filament C alone. This was consistent with the spectral line enhancement with double-pulse plasma excitations.

As the interpulse delay was set at -50 ps, conceptually different nonlinear couplings occurred between the plasma gratings and filament of pulse C. The top view of the noncollinear interaction area between the ahead pulse C (-50 ps delay) and plasma grating induced by pulses A and B is shown in Fig. 5. In this case, pulse C experienced filamentation at first that created self-guiding plasma channels of about $100\text{-}\mu\text{m}$ -diameter in air, which in turn made the fluid jet and air–aqueous interface be ablated, i.e., filament excitation occurred at first. Although the femtosecond laser pulses were temporarily confined within the pulse duration (e.g., about 40 fs in our experiments), the plasma channel typically lasted tens of picoseconds, which helped to effectively improve the plasma density of filaments formed later. It has been well demonstrated that there existed observable nonlinear interactions among delayed filaments.⁶² When synchronized pulses A and B overlapped upon the filament channels as-formed by pulse C, both pulses A and B established their own filaments under the circumstance of the already existed plasma from the ahead pulse C, plasma defocusing effects were altered and laser self-focusing should be changed accordingly to reach a new region of balance. Consequently, filaments of pulses A and B interfered differently in the presence of plasma defocusing from the ahead pulse C, and nonlinear filament interactions resulted in the formation of plasma gratings under the influence of the still-lasted plasma channels of the ahead filament C. Plasma grating ablation and excitation were also reasonably different from that without filament C. As plasma gratings were established with additional plasma defocusing from the ahead pulse C, their electron densities were further increased, plasma ablation and excitation efficiency of the liquid sample was thus further improved. Appropriate delay at -50 ps for the best spectral line enhancement implied that

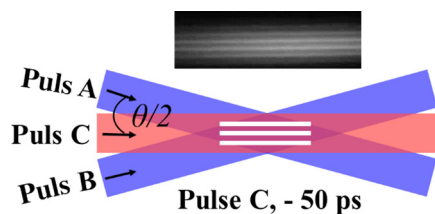


Fig. 5 Top view of the noncollinear interaction area between the ahead pulse C (-50 ps delay) and plasma grating inducing by pulses A and B.

plasma gratings were best formed under properly expanded plasma channels of the ahead pulse C. This was consistent with the fact that plasma gratings were established in an area larger than the well-confined single filaments, and that the as-formed filamentation channels with an approximately lifetime duration of plasma expansion could support better filament interactions of pulses A and B.

As all the three filaments were synchronized and shown in Fig. 6, their interactions generated novel kinds of plasma gratings that exhibited quite different microplasma structures. As the synchronized pulse C participated the coplanar noncollinear interference in the cross-overlapped region, the interference patterns differed from that of two noncollinear fs laser beams (pulses A and B), and thus plasma gratings were formed in accordance with the change of interference patterns, giving rising to periodic plasma channels of fine structures in which electron density and peak intensity could be further enhanced using more synchronized pulses to interfere noncollinearly.

3.3 Signal Enhancements of Breakdown Spectral Lines

To further analyze the plasma breakdown enhancements, we used GIBS (pulse A and pulse B, total laser energy at 1.4 mJ) and FIBS (pulse C, total laser energy at 0.6 mJ) techniques to acquire spectral line signals, respectively, to compare with F-GIBS (total laser energy at 2.0 mJ). Figure 7 shows the comparison results in which Figs. 7(a)–7(d) represent the spectral lines of the Cu, Cr, H, and Na elements, respectively. FIBS hardly excited aqueous solutions, as indicated by blue curves in Figs. 7(a)–7(d), almost no obvious spectral line signals were observed, except for the easily excited Na element. FIBS spectral lines could not increase further as the input fs laser energy was adjusted to reach a saturated excitation, indicating that filaments and the accompanied filament excitations reached peak-intensity-clamping limits. In all aqueous solutions containing small amounts of elements, filamentation was mainly limited by the optical nonlinearity of water as the major constituent, and plasma channels generated therein could guide laser pulses without filamentation breakups of much lower peak intensities than those in air. As a distinct contrast to FIBS, GIBS spectral line intensities were significantly improved, and all elements (Cu, Cr, and Na) were excited to emit sharp spectral lines. The GIBS protocol allowed for further increase of laser energies (pulses A and B) beyond the intensity clamping limits of single filaments and exhibited the pronounced advantage in evading breakups of the plasma grating channels in the fluid jet stream. In air, fs laser pulses were tightly guided in the plasma gratings, the nonlinearly coupled filaments (pulses A and B) entered the fluid jet through the air–aqueous interface and established plasma gratings in the aqueous solutions, which excited the fluid jet completely differently from single filaments alone. As all the

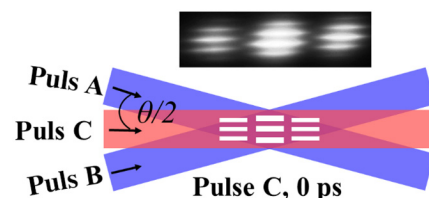


Fig. 6 Top view of the noncollinear coplanar filament interaction area as the three filaments are synchronized.

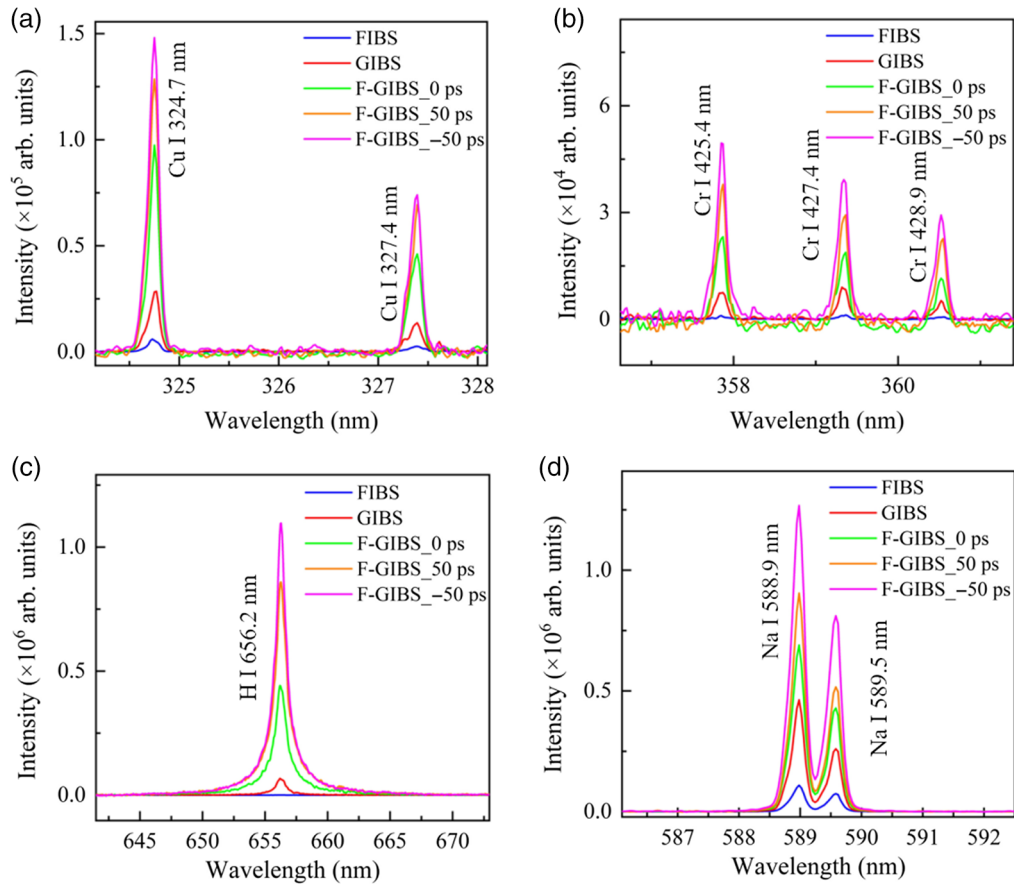


Fig. 7 Comparison of FIBS, GIBS, and F-GIBS at different delays (0 and ± 50 ps) in aqueous solutions for spectral lines of (a) Cu, (b) Cr, (c) H, and (d) Na elements.

three pulses A, B, and C were synchronized to excite the liquid samples (F-GIBS at 0 ps), an interesting phenomenon was observed. The spectral line intensities were significantly improved, much greater than the summation of FIBS and GIBS. In addition, further spectral line signal enhancement occurred when the interpulse delay was about -50 ps (F-GIBS at -50 ps) and 50 ps (F-GIBS at 50 ps), respectively. It should be noted that at these interpulse delays, the filament formed by pulse C did not interact directly with the other filaments. However, as aforementioned, the plasma grating formed by the interference of pulses A and B exhibited different nonlinear couplings with filaments formed by pulse C at positive or negative delays, to achieve better excitation and improved spectral line signals.

In order to better compare the spectral line emission differences and effects arisen from nonlinear couplings of filaments with plasma gratings in different excitation protocols, we define the ratio of the spectral line intensities of GIBS and F-GIBS versus FIBS as the enhancement factors: $E_{\text{GIBS}} = I_{\text{GIBS}}/I_{\text{FIBS}}$ and $E_{\text{F-GIBS}} = I_{\text{F-GIBS}}/I_{\text{FIBS}}$, where I_{FIBS} , I_{GIBS} , and $I_{\text{F-GIBS}}$ denote the spectral line intensity attained with FIBS, GIBS, and F-GIBS, respectively. Filament excitations induced quite low breakdown emissions in liquids, and beyond the filamentation threshold, FIBS did not increase any more by merely increasing the excitation pulse energy due to the peak-intensity clamping of single filaments,^{46,50} i.e., I_{FIBS} reached saturation under filament excitation and even worse, single filaments randomly broke up into multiple filaments in liquids as the

excitation pulse energy increased further. Although in GIBS and F-GIBS, laser pulses were confined in the plasma grating channels and total pulse energy could be increased beyond the filament breakup limits. The enhancement factors calculated from the measured spectra are summarized in Table 1. As FIBS was replaced by GIBS, two synchronized pulses with a total energy of 1.4 mJ entered the aqueous solutions; instead of multifilamentation breakup, plasma gratings were formed. $I_{\text{GIBS}}/I_{\text{FIBS}}$ ranged from 3 to 5 for Cu and Na elements and reached more than 22 for the Cr element. This enhancement could be ascribed to the enhanced peak intensity and plasma density in the as-formed plasma gratings. By coupling the third filament into the plasma gratings, F-GIBS achieved more prominent enhancements. At the interpulse delay of 0 ps, F-GIBS intensities were enhanced about 6, 28, and 99 times for Na, Cu, and Cr elements, respectively. At the interpulse delay of ± 50 ps (i.e., F-GIBS at ± 50 ps), nonlinear couplings between the filament and plasma gratings further enhanced the spectral lines of Na, Cu, and Cr elements up to 12, 87, and 195 times, respectively. Note that F-GIBS at -50 ps was slightly larger than that at 50 ps and that the asymmetric enhancement was pronounced for the Na element. This could be readily understood by the mechanism difference of nonlinear couplings between the third filament and the plasma gratings under positive and negative delays. In addition, the measured enhancement factors differed among the three elements tested in our experiments, which may be mainly related to the reactivity difference

Table 1 The enhancement factors of various spectral lines attained by GIBS and F-GIBS excitation protocols versus FIBS.

Line	E_1 to E_2 (eV)	E_{GIBS}	$E_{\text{F-GIBS}}$		
			0 ps	50 ps	-50 ps
Cu I 324.7 nm	0.000 to 3.816	3.19	26.38	70.36	77.71
Cu I 327.4 nm	0.000 to 3.785	5.11	28.33	75.31	87.62
Cr I 425.4 nm	0.000 to 2.913	22.03	92.80	145.77	174.98
Cr I 427.4 nm	3.086 to 5.986	18.08	94.72	154.52	177.99
Cr I 428.9 nm	0.000 to 2.889	20.59	99.11	152.71	195.18
Na I 588.9 nm	0.000 to 2.104	4.51	6.75	8.87	12.44
Na I 589.5 nm	0.000 to 2.102	3.58	5.91	7.19	11.21

of elements. F-GIBS contained efficient multiphoton excitations directly from fs laser pulses as well as electron collisions in the elongated plasma gratings, nonlinear couplings of filaments with plasma gratings hence induced prominent enhancements of breakdown emissions for heavy metal elements, such as Cu and Cr, that require high laser intensity and electron density to excite.

4 Conclusions

Laser ablation has been well-developed as a basic tool in trace element analysis, material processing, and surface treating. So far, it is still a great challenge to implement efficient laser ablation on or inside liquids, as plasma excitations therein are limited by unavoidable generation of shockwaves and micro-bubbles, as well as rapid plasma annihilation intrinsically accompanied by a dramatic liquid pressure change surrounding the ablation region. In this work, we built an F-GIBS system and implemented with the method of creating fluid jets to analyze aqueous solutions. Two fs laser beams were noncollinearly coupled to establish plasma gratings covering almost the entire jet to excite the liquid sample, and a third filament was aligned to nonlinearly coupled with the plasma gratings in the same plane (vertical to the fluid jet). This kind of plasma excitation manifested as a dexterous technique that smartly avoided detrimental influence from liquid surface fluctuation and bubbles formed by the violent plasma explosion. It is intriguing to note that nonlinearly coupled filaments entered the fluid jet across the air–aqueous interface with no random filament breakups. Three synchronized filaments established plasma grating structures determined by their interference patterns, enhancing the F-GIBS signals, much greater than the summation of those attained by FIBS and GIBS alone. More prominent enhancements of F-GIBS were observed as the third filament was delayed at ± 50 ps. Even though laser pulses guided in the third filament did not interact directly with those in the plasma gratings at these delays, the corresponding filaments still experienced strong nonlinear couplings. Such nonsimultaneous nonlinear couplings supported plasma excitations conceptually different from the traditional double-pulse excitation. We found that different metal elements were excited with distinct spectral line improvements and up to 195 times enhancement was attained for F-GIBS spectral line Cr I 428.9 nm as compared to that induced by filament (FIBS). Our experimental observations validated that coplanar interaction of filaments and plasma gratings efficiently excited vertical fluid jets in such a way that it not only

overcame side effects from plasma-grating generated bubbles but also dramatically increased the plasma excitations and evaded random multiple filamentation breakup across the air–aqueous interfaces. F-GIBS provides a promising technique for trace element detection in aqueous solutions with improved sensitivities. Regenerative excitations of plasma gratings demonstrated in this work pave a way to include with merits of some other already well-developed DP-LIBS techniques, such as plasma reheating¹⁴ and laser induced fluorescence,¹⁵ with resonant re-excitation in much shorter time delays, facilitating convenient use of lasers from the same sources.

Acknowledgments

This work was sponsored by Shanghai Rising-Star Program (Grant No. 22QC1401000), the National Defense Administration of Science, Technology and Industry (Grant No. HTKJ2021KL504014), the National Key Research and Development Program (Grant No. 2018YFB0504400), the National Natural Science Foundation of China (Grant Nos. 11621404, 11727812, and 62035005), and Shanghai Municipal Science and Technology Major Project (Grant No. 2019SHZDZX01-ZX05).

Code, Data, and Materials Availability

The data that support the findings of this study are available from the corresponding author upon reasonable request.

References

1. A. Ym et al., “Laser opto-ultrasonic dual detection for simultaneous compositional, structural, and stress analyses for wire + arc additive manufacturing,” *Addit. Manuf.* **31**, 100956 (2020).
2. Z. A. Deng et al., “A plasma-image-assisted method for matrix effect correction in laser-induced breakdown spectroscopy,” *Anal. Chim. Acta* **1107** 14–22 (2020).
3. L. B. Guo et al., “Development in the application of laser-induced breakdown spectroscopy in recent years: a review,” *Front. Phys.* **16**(2), 22500 (2021).
4. C. R. Bhatt et al., “Evaluation of analytical performance of double pulse laser-induced breakdown spectroscopy for the detection of rare earth elements,” *Opt. Laser Technol.* **126**, 106110 (2020).
5. B. Li et al., “A review of femtosecond laser-induced emission techniques for combustion and flow field diagnostics,” *Appl. Sci.* **9** (9), 1906 (2019).
6. Y. Wenbin et al., “Quantitative analysis of trace oxygen concentration in argon and nitrogen based on laser-induced breakdown spectroscopy,” *Chin. J. Lasers* **44**(10), 1011001 (2017).

7. V. Sturm and R. Noll, "Laser-induced breakdown spectroscopy of gas mixtures of air, CO₂, N₂, and C₃H₈ for simultaneous C, H, O, and N measurement," *Appl. Opt.* **42**(30), 6221–6225 (2003).
8. L. Zheng et al., "On the performance of laser-induced breakdown spectroscopy for direct determination of trace metals in lubricating oils," *Spectrochim. Acta, Part B* **99**(1), 1–8 (2014).
9. C. Du, C. Yang, and M. Zhang, "Investigation on the dynamic characteristics of LIBS for heavy metal Mn in liquid matrix," *Optik* **180**, 602–609 (2019).
10. V. Lazic and S. Jovičević, "Laser induced breakdown spectroscopy inside liquids: processes and analytical aspects," *Spectrochim. Acta, Part B* **101**, 288–311 (2014).
11. Y. Chu et al., "Half-life determination of inorganic-organic hybrid nanomaterials in mice using laser-induced breakdown spectroscopy," *J. Adv. Res.* **24**, 353–361 (2020).
12. P. A. Babushkin, G. G. Matvienko, and V. K. Oshlakov, "Determination of the elemental composition of aerosol by femtosecond laser-induced breakdown spectroscopy," *Atmos. Ocean. Opt.* **35**(1), 19–26 (2022).
13. L. M. Narlagiri et al., "Recent trends in laser-based standoff detection of hazardous molecules," *TrAC Trends Anal. Chem.* **153**, 116645 (2022).
14. X. Pu and N. H. Cheung, "ArF laser induced plasma spectroscopy of lead ions in aqueous solutions: plume reheating with a second Nd:YAG laser pulse," *Appl. Spectrosc.* **57**(5), 588–590 (2003).
15. H. Loudyi et al., "Improving laser-induced breakdown spectroscopy (LIBS) performance for iron and lead determination in aqueous solutions with laser-induced fluorescence (LIF)," *J. Anal. At. Spectrom.* **24**(10), 1421–1428 (2009).
16. S. Niu, L. Zheng, and H. Zeng, "Laser sintered adsorption of metal elements on oxide nanoparticles for laser induced breakdown spectroscopic analysis of solid," *Spectrochim. Acta, Part B* **158**(1), 105626 (2019).
17. A. K. S. Ajmathulla and V. R. Soma, "Discrimination of bimetallic alloy targets using femtosecond filament-induced breakdown spectroscopy in standoff mode," *Opt. Lett.* **43**(15), 3465–3468 (2018).
18. A. K. Shaik and V. R. Soma, "Standoff discrimination and trace detection of explosive molecules using femtosecond filament induced breakdown spectroscopy combined with silver nanoparticles," *OSA Contin.* **2**(3), 554–562 (2019).
19. D. Zhang et al., "Three-dimensional elemental imaging of material surface using image-assisted laser-induced breakdown spectroscopy," *Appl. Surf. Sci.* **534**, 147601 (2020).
20. P. J. Skrodzki, M. Burger, and I. Jovanovic, "Transition of femtosecond-filament-solid interactions from single to multiple filament regime," *Sci. Rep.* **7**, 12740 (2017).
21. A. K. Shaik et al., "Femtosecond laser induced breakdown spectroscopy based standoff detection of explosives and discrimination using principal component analysis," *Opt. Express* **26**(7), 8069–8083 (2018).
22. D. C. Zhang et al., "Simple method for liquid analysis by laser-induced breakdown spectroscopy (LIBS)," *Opt. Express* **26**(14), 18794–18802 (2018).
23. Y. Jing et al., "Research about analysis of heavy metals in liquid jet by laser-induced breakdown spectroscopy," *Chin. J. Lasers* **39**(2), 0215001 (2012).
24. D. Zhu et al., "Laser-induced breakdown spectroscopy for determination of trace metals in aqueous solution using bamboo charcoal as a solid-phase extraction adsorbent," *Anal. Methods* **4**(3), 819–823 (2012).
25. D. Bae et al., "Spreading a water droplet on the laser-patterned silicon wafer substrate for surface-enhanced laser-induced breakdown spectroscopy," *Spectrochim. Acta, Part B* **113**, 70–78 (2015).
26. H. Sobral, R. Sanginés, and A. Trujillo-Vázquez, "Detection of trace elements in ice and water by laser-induced breakdown spectroscopy," *Spectrochim. Acta, Part B* **78**, 62–66 (2012).
27. C. Wang et al., "Enrichment of trace lead in water with graphite and measurement by laser-induced breakdown spectroscopy," *Chin. J. Lasers* **38**(11), 1115002 (2011).
28. S. Niu et al., "Laser-induced breakdown spectroscopic detection of trace level heavy metal in solutions on a laser-pretreated metallic target," *Talanta* **179**(1), 312–317 (2018).
29. L. Zheng et al., "Comparative study of the matrix effect in Cl analysis with laser-induced breakdown spectroscopy in a pellet or in a dried solution layer on a metallic target," *Spectrochim. Acta, Part B* **118**, 66–71 (2016).
30. B. Xue et al., "Characteristics of the secondary breakdown of DP-LIBS in bulk water with different axial focusing arrangements and laser energies," *Spectrochim. Acta, Part B* **151**, 20–25 (2019).
31. M. L. Zheng et al., "Quantitative analysis of Cu in water by collinear DP-LIBS," *Spectrosc. Spectral Anal.* **34**(7), 1954–1958 (2014).
32. Y. Feng et al., "Investigation of laser-induced breakdown spectroscopy of a liquid jet," *Appl. Opt.* **49**(13), C70–C74 (2010).
33. K. L. Eland et al., "Energy dependence of emission intensity and temperature in a LIBS plasma using femtosecond excitation," *Appl. Spectrosc.* **55**(3), 286–291 (2001).
34. P. J. Skrodzki et al., "Ultrafast laser filament-induced fluorescence spectroscopy of uranyl fluoride," *Sci. Rep.* **8**, 11629 (2018).
35. S. S. Harilal et al., "Consequences of femtosecond laser filament generation conditions in standoff laser induced breakdown spectroscopy," *Opt. Express* **24**(16), 17941–17949 (2016).
36. E. L. Gurevich and R. Hergenröder, "Femtosecond laser-induced breakdown spectroscopy: physics, applications, and perspectives," *Appl. Spectrosc.* **61**(10), 233A–242A (2007).
37. A. Couairon and A. Mysyrowicz, "Femtosecond filamentation in transparent media," *Phys. Rep.* **441**(2–4), 47–189 (2007).
38. Y. H. Chen et al., "Direct measurement of the electron density of extended femtosecond laser pulse-induced filaments," *Phys. Rev. Lett.* **105**(21), 215005 (2010).
39. N. Li et al., "Signal enhancement in underwater long-pulse laser-induced breakdown spectroscopy for the analysis of bulk water," *J. Anal. At. Spectrom.* **36**(6), 1170–1179 (2021).
40. M. Cui et al., "Signal improvement for underwater measurement of metal samples using collinear long-short double-pulse laser induced breakdown spectroscopy," *Front. Phys.* **8**, 237 (2020).
41. F. Liu et al., "Filamentary plasma grating induced by interference of two femtosecond laser pulses in water," *Opt. Express* **25**(19), 22303–22311 (2017).
42. H. Peng et al., "Dynamical aspects of plasma gratings driven by a static ponderomotive potential," *Plasma Phys. Control. Fusion* **62**(11), 115015 (2020).
43. S. E. Schrauth et al., "Study of self-diffraction from laser generated plasma gratings in the nanosecond regime," *Phys. Plasmas* **26**(7), 073108 (2019).
44. M. Li et al., "Particle in cell simulation on plasma grating contrast enhancement induced by infrared laser pulse," *Phys. Plasmas* **25**(5), 053106 (2018).
45. J. Liu et al., "Two-dimensional plasma grating by non-collinear femtosecond filament interaction in air," *Appl. Phys. Lett.* **99**(15), 151105 (2011).
46. M. Y. Hu et al., "Plasma-grating-induced breakdown spectroscopy," *Adv. Photonics* **2**(6), 065001 (2020).
47. P. Lu, J. Wu, and H. Zeng, "Manipulation of plasma grating by impulsive molecular alignment," *Appl. Phys. Lett.* **103**(22), 221113 (2013).
48. X. Yang et al., "Experimental observation of noncollinear coupling of filaments in air," in *Proc. CLEO 2008 Tech. Conf.*, IEEE, San Jose, California, p. CTuE6 (2008).
49. X. Yang et al., "Plasma waveguide arrays from filament interaction in air," in *Conf. Lasers and Electro-Opt. 2010 OSA Tech. Digest (CD)*, Optical Society of America, San Jose, California, p. CTuPPI (2010).

50. M. Hu et al., “Femtosecond laser-induced breakdown spectroscopy by multidimensional plasma grating,” *J. Anal. At. Spectrom.* **37**(4), 841–848 (2022).
51. C. B. Faye, E. Frejafon, and T. Amodeo, “Sampling considerations when analyzing micrometric-sized particles in a liquid jet using laser induced breakdown spectroscopy,” *Spectrochim. Acta, Part B* **91**(1), 5–11 (2014).
52. S. Koch et al., “Resonance fluorescence spectroscopy in laser-induced cavitation bubbles,” *Anal. Bioanal. Chem.* **385**(2), 312–315 (2006).
53. S. Koch et al., “Detection of manganese in solution in cavitation bubbles using laser induced breakdown spectroscopy,” *Spectrochim. Acta, Part B* **60**(7), 1230–1235 (2005).
54. X. Yang et al., “Femtosecond laser pulse energy transfer induced by plasma grating due to filament interaction in air,” *Appl. Phys. Lett.* **97**(7), 071108 (2010).
55. L. Shi et al., “Generation of high-density electrons based on plasma grating induced Bragg diffraction in air,” *Phys. Rev. Lett.* **107**(9), 095004 (2011).
56. Z. Wang et al., “Emission characteristics of laser-induced plasma using collinear long and short dual-pulse laser-induced breakdown spectroscopy (LIBS),” *Appl. Spectrosc.* **71**(9), 2187–2198 (2017).
57. M. Cui et al., “Carbon detection in solid and liquid steel samples using ultraviolet long-short double pulse laser-induced breakdown spectroscopy,” *Spectrochim. Acta, Part B* **167**, 105839 (2020).
58. R. Yang and L. Bi, “Spectral enhancement mechanism and analysis of defocused collinear DP-LIBS technology,” *Optik* **243**, 167025 (2021).
59. S. S. Harilal, J. Yeak, and M. C. Phillips, “Plasma temperature clamping in filamentation laser induced breakdown spectroscopy,” *Opt. Express* **23**(21), 27113–27122 (2015).
60. L. A. Finney et al., “Filament-induced breakdown spectroscopy signal enhancement using optical wavefront control,” *Opt. Commun.* **490**(1), 126902 (2021).
61. H. W. Zang et al., “In situ determination of the equivalence ratio in a methane/air flow field by femtosecond filament excitation,” *Laser Phys.* **30**(3), 035402 (2020).
62. D. Reyes et al., “Filament conductivity enhancement through nonlinear beam interaction,” *Opt. Express* **28**(18), 26764–26773 (2020).

Mengyun Hu received her MS degree from the East China Normal University in 2014. In the same year, she joined the State Key Laboratory of Precision Spectroscopy of the East China Normal University, as an engineer. She has participated in the National Key Research and Development Program of China. She was selected as Shanghai Rising-Star.

Her current research interests are in precision spectral detection and applications.

Fangfang Li received her PhD in physical chemistry from Fudan University in 2020. In the same year, she conducted postdoctoral research at Fudan University. In 2022, she joined the State Key Laboratory of Precision Spectral Science and Technology of East China Normal University as a full-time associate researcher. Her current research focuses on precise spectral detection and applications, particularly in laser-induced breakdown spectroscopy.

Shencheng Shi received his MS degree from the State Key Laboratory of Precision Spectroscopy of the East China Normal University in 2022. His main research interest was ultrafast laser-induced breakdown spectroscopy, which is an improved technology of laser induced breakdown spectroscopy based on ultrafast laser technology such as filament and plasma grating.

Yu Qiao graduated from Hunan Normal University in 2018 and joined the State Key Laboratory of Precision Spectral Science and Technology of East China Normal University as a master's student in the following year, and starts his PhD in 2021 in the same lab. His current research is focused on precision spectral detection and applications, with a particular focus on laser-induced breakdown spectroscopy.

Jinman Ge received her PhD in optical engineering from Nanjing University of Science and Technology, Nanjing, China, in 2018. She is a postdoctoral fellow of the National Key Laboratory of Science and Technology on Space Microwave and works at Xi'an Branch of the China Academy of Space Technology, China. Her research interests include space laser communication, optical phased array antennas, and optical precision measurement technology.

Xiaojun Li received his PhD from Xidian University. He is a professor of the National Key Laboratory of Science and Technology on Space Microwave, China Academy of Space Technology, Xi'an, Shaanxi, China. He is a senior member of China Communication Society. His research focus on innovative technology of space microwaves, wireless energy transfer in space, and THz communication.

Heping Zeng received his PhD from Shanghai Institute of Optics and Fine Mechanics at the Chinese Academy of Sciences. He is a professor of the State Key Laboratory of Precision Spectroscopy, East China Normal University, Shanghai, China. He was selected as a distinguished young scholar of NSFC. He was invited to serve as an editorial board member for *European Physical Journal D*. He is a fellow of OSA. His research focuses on precision control of the light field and its application in precision spectroscopy.